Journal of Molecular Catalysis A: Chemical 398 (2015) 391–398

Contents lists available at ScienceDirect

Journal of Molecular Catalysis A: Chemical

journal homepage: www.elsevier.com/locate/molcata

Promoting effect of WO_x on selective hydrogenolysis of glycerol to 1,3-propanediol over bifunctional Pt–WO_x/Al_2O_3 catalysts

Shanhui Zhu[a,*], Xiaoqing Gao[b], Yulei Zhu[a,b,*], Yongwang Li[a,b]

[a] State Key Laboratory of Coal Conversion, Institute of Coal Chemistry, Chinese Academy of Sciences, Taiyuan 030001, PR China
[b] Synfuels China Co., Ltd, Taiyuan 030032, PR China

ARTICLE INFO

Article history:
Received 10 November 2014
Received in revised form
24 December 2014
Accepted 29 December 2014
Available online 31 December 2014

Keywords:
Glycerol
Hydrogenolysis
1,3-Propanediol
WO_x
Pt

ABSTRACT

Despite 1,3-propanediol possessing high economic value, its production from glycerol hydrogenolysis is a challenging task. Herein, a series of WO_x promoted Pt/Al_2O_3 catalysts with various WO_x contents were prepared and investigated for selective production 1,3-propanediol from glycerol hydrogenolysis. To explore the structure feature, these catalysts were fully characterized by BET, CO chemisorption, HRTEM, XRD (*in situ* XRD), Raman, NH_3–TPD, Py–IR, H_2–TPR, and XPS. Among them, Pt–10WO_x/Al_2O_3 achieved the highest 1,3-propanediol yield up to 42.4%, which was ascribed to the large concentration of Brønsted acid sites, strong electronic interaction between Pt with WO_x and hydrogen spillover. The strong correlation between 1,3-propanediol yield and Brønsted acid site indicated its essential role for the formation of 1,3-propanediol. Meanwhile the linear correlation between 1,2-propanediol yield and Lewis acid site gave direct evidence that Lewis acid site preferentially generated 1,2-propanediol.

1. Introduction

The use of renewable resources as feedstocks for the production of fuels, chemicals and materials has been attracting much attention, as the fossil resources will be exhausted in a few decades [1,2]. In this context, biomass is a desirable candidate as an alternative and carbon neutral resource. As a biomass-derivative, glycerol is currently produced in a large amount as a by-product in manufacturing biodiesel by transesterification of vegetable oils with methanol or ethanol [3]. Therefore, it is urgent to effectively utilize the renewable glycerol for the sustainable development of biodiesel industry. Significant research efforts have been focused on the transformation of glycerol by various catalytic processes, such as reforming [4], oxidation [5], dehydration [6], hydrogenolysis [7,8], esterification [9,10] and polymerization [11].

The catalytic hydrogenolysis of glycerol to 1,2-propanediol (1,2-PDO) and 1,3-propanediol (1,3-PDO), which are widely used as versatile specialty chemicals, is quite promising. 1,3-PDO owes much higher economic value than 1,2-PDO, in particular, as an important monomer in the synthesis of polyester fibers [7]. Conversion of glycerol to 1,2-PDO has been extensively studied, and high yields have been obtained in previous reports [12–15]. Our recent work has achieved 98.0% yield of 1,2-PDO over B_2O_3 modified Cu/SiO_2 catalyst [15]. On the contrary, the direct hydrogenolysis of glycerol to 1,3-PDO is still a challenging task. One of the key problems is concerned with the 1,3-PDO selectivity, which requires careful design of catalyst.

There have been several reports on homogeneous and heterogeneous catalysts for the catalytic hydrogenolysis of glycerol to 1,3-PDO [16–21]. Nevertheless, most of previous studies have been performed in organic solvent [16,19,22]. Considering that crude glycerol from biodiesel production contains water unavoidably and it is also a by-product of the reaction sequence, water is the desired solvent for glycerol hydrogenolysis from the standpoint of environmental and economic viability. Among them, the relatively effective processes using water primarily employed Ir–ReO_x/SiO_2 [20,23] or Pt-based catalysts modified by tungsten species (WO_3 [16,24], WO_x [21,25], H_2WO_4 [22] and $H_4SiW_{12}O_{40}$ [26,27]). Nakagawa et al. developed Ir–ReO_x/SiO_2 catalyst with H_2SO_4 as an additive in a batch reactor, over which the yield of 1,3-PDO reached 38% [20]. To overcome the corrosive liquid H_2SO_4, H-ZSM-5 was considered as the most suitable solid acid co-catalyst and the yield of 1,3-PDO declined to 33% moderately [23]. Zhang et al. [21] performed glycerol hydrogenolysis over mesoporous WO_3–TiO_2 with a loading of 2 wt% Pt at 180 °C and 5.5 MPa, which gave 40.3% 1,3-PDO selectivity and 24.2% conversion. Qin et al. [24] achieved 32.0% yield of 1,3-PDO over Pt/WO_3/ZrO_2 catalyst in glycerol hydrogenolysis at 130 °C and 4 MPa. The other relatively feasible catalysts included Pt/WO_3/TiO_2/SiO_2 [28], Pt-$H_4SiW_{12}O_{40}$/ZrO_2

* Corresponding author. Tel.: +86 351 7117097.
E-mail addresses: zhushanhui@sxicc.ac.cn (S. Zhu), zhuyulei@sxicc.ac.cn (Y. Zhu).

http://dx.doi.org/10.1016/j.molcata.2014.12.021
1381-1169/

[27,29], $Pt/Al_2O_3 + H_4SiW_{12}O_{40}$ [26], Pt/WO_x/Boehmite [25], and $Pt/WO_x/SiO_2/ZrO_2$ [30]. These results show that the acidic tungsten species appear as a key to the selective formation of 1,3-PDO, but the role of tungsten species is still unclear. Despite growing experimental work, a systematic understanding remains unavailable on the type of acid sites in governing the rate and cleavage C—O bond selectively over tungsten-containing catalysts.

In the present work, we reported a detailed study for continuous hydrogenolysis of glycerol over Pt-WO_x/Al_2O_3 catalysts in aqueous media. A 42.4% yield of 1,3-PDO was achieved at 64.2% conversion, 160 °C and 5.0 MPa over Pt–$10WO_x/Al_2O_3$ catalyst. Special emphasis would be focused on the role of WO_x and structure-behavior correlation.

2. Experiment

2.1. Catalyst preparation

The Pt–WO_x/Al_2O_3 catalysts were prepared by sequential impregnation method. Specifically, γ-Al_2O_3 (China Research Institute of Daily Chemical Industry) was impregnated with aqueous solutions containing the desired amount of ammonium paratungstate (Sinopharm Chemical Reagent Co., Ltd., China, (SCRC)). These WO_x/Al_2O_3 samples were dried overnight at 110 °C and calcined at 600 °C in static air for 4 h. The Pt–WO_x/Al_2O_3 catalysts were fabricated by impregnation of WO_x/Al_2O_3 samples with an aqueous solution of $H_2PtCl_6{\cdot}6H_2O$ (SCRC). Impregnated samples were dried overnight at 110 °C and then calcined in static air at 400 °C for 4 h. According to the tungstate oxide mass (y in wt%, quantified in the form of WO_3), the final catalysts were designated as Pt–yWO_x/Al_2O_3 ($y = 5 \sim 20$). The Pt/Al_2O_3 without WO_x was also prepared as reference sample by impregnation of γ-Al_2O_3 with an aqueous solution of $H_2PtCl_6{\cdot}6H_2O$. The Pt/Al_2O_3 sample was dried and then calcined at 400 °C for 4 h. The loading of Pt were fixed at 2 wt% in all catalysts.

2.2. Catalyst characterization

N_2 adsorption–desorption isotherms were recorded at −196 °C on a Micromeritics ASAP 2420 instrument. Prior to the measurement, each sample was degassed under vacuum at 300 °C for 8 h.

Powder X-ray diffraction (XRD) patterns were collected on a D2/max-RA X-ray diffractometer (Bruker, Germany) with Cu Kα radiation operated at 30 kV and 10 mA. The X-ray patterns were recorded in 2θ values ranging from 10° to 90°. For *in situ* XRD measurement, these samples were flushed in pure H_2 at a flow rate of 30 $cm^3\ min^{-1}$ and heated from 30 °C to 150, 250, 300, 350, 400, 450, 500, 550 and 600 °C at a ramping rate of 5 °C min^{-1}. The XRD patterns were recorded after the preset temperature attained for 30 min.

Transmission electron microscopy (TEM) and high-resolution transmission electron microscopy (HRTEM) images of the samples were obtained in JEM 2011F apparatus operating at 200 kV voltages. The samples after reduction were suspended in ethanol with an ultrasonic dispersion for 30 min and deposited on carbon-coated copper grids.

Raman spectroscopy was conducted on a LabRAM HR800 System using a CCD detector at room temperature. The 325 nm of the He–Cd laser was employed as the exciting source with a power of 30 MW.

CO chemisorption was performed in Auto Chem. II 2920 equipment (Mircromeritics, USA). Prior to adsorption measurement, 0.2 g catalyst sample was reduced in H_2 for 2 h at 200 °C and then flushed with He for 1 h followed by cooling down to 30 °C. The CO chemisorption was measured by pulse injection of pure CO at 30 °C. The Pt particle size was determined by assuming that the stoichiometry of adsorbed CO molecule to surface platinum atom was one.

Temperature-programmed reduction of hydrogen (H_2–TPR) was conducted in the same apparatus as CO chemisorption. For each run, about 0.10 g sample was firstly pretreated in Ar at 150 °C for 30 min and then cooled to 30 °C. After that, 10% H_2 diluted in Ar was introduced into the system and a cold trap of 2-propanol-liquid nitrogen slurry was provided to condense the water gas. The sample was heated up to 900 °C at a ramp of 10 °C/min and simultaneously recorded by a thermal conductivity detector.

Temperature-programmed desorption of ammonia (NH_3–TPD) was measured in the same apparatus as CO chemisorption. At first, 0.3 g catalyst sample was pretreated in He at 400 °C for 1 h and then cooled to 100 °C followed by saturating with pure NH_3 for 30 min. Finally, the sample was heated to 600 °C at a ramping rate of 10 °C/min and the desorbed NH_3 was monitored with a MS detector (Agilent, USA).

IR spectra of adsorbed pyridine (Py–IR) were performed in Vertex 70 (Bruker) FT-IR spectrophotometer with a deuterium triglycine sulfate (DTGS) detector. For each run, the sample was pressed into self-supporting wafers and degassed in vacuum at 300 °C for 1 h followed by exposure to pyridine vapor. Subsequently, the Py–IR spectra were measured at 200 °C after applying vacuum for 30 min. The quantification of Brønsted and Lewis acid sites was estimated from the integrated area of adsorption bands at *ca.* 1540 and 1450 cm^{-1}, respectively, described elaborately in our previous reports [10,27].

X-ray photoelectron spectroscopy (XPS) was carried out on a VG MiltiLab 2000 spectrometer with Mg Kα radiation and a multichannel detector. The catalyst was reduced in flowing hydrogen at 200 °C for 2 h before the measurement. The obtained binding energy values were calibrated by the C 1s peak at 284.6 eV.

2.3. Catalytic reaction

The catalytic test was performed in a vertical fixed-bed stainless steel reactor with an ice–water trap. Typically, 2.0 g catalyst (20–40 mesh) was placed into the constant temperature section of the reactor possessing quartz sand to fix it in both ends. Prior to the test, the catalyst was reduced in flowing H_2 (100 ml/min) at 200 °C for 2 h. Subsequently, a glycerol aqueous solution (1.8 ml/h) was continuously pumped into the reactor inlet through an HPLC pump. The liquid and gas products were condensed and collected in a gas–liquid separator immersed in an ice–water trap. The standard reaction conditions were as follows: 160 °C, 5.0 MPa, 10 wt% glycerol aqueous solution, H_2/glycerol = 137:1 (molar ratio), WHSV = 0.09 h^{-1}.

The liquid products were analyzed by a gas chromatography (Ruihong chromatogram analysis Co., Ltd., China) with a FID using a DB-WAX capillary column. The outlet gas was off-line analyzed using a gas chromatograph (Huaai chromatogram analysis Co., Ltd., China) equipped with a TCD and OV-101 column. Concurrently, the assignment of the products was identified by GC–MS (Agilent, USA).

The identified products were 1,3-PDO, 1,2-PDO, 1-propanol (1-PO), 2-propanol (2-PO), ethanol, acetol, propionic acid, acetic acid, ethylene glycol, methanol, propane, methane and CO_2. The conversion of glycerol and selectivity of products were calculated using the following expressions:

$$\text{Conversion}(\%) = \frac{\text{moles of glycerol(in)} - \text{moles of glycerol(out)}}{\text{moles of glycerol(in)}} \times 100$$

$$\text{Selectivity}(\%) = \frac{\text{moles of one product}}{\text{moles of all products}} \times 100$$

Table 1
Physicochemical properties and acidities of Pt/Al_2O_3 and $Pt–WO_x/Al_2O_3$ catalysts.

Catalyst	Surface area ($m^2\ g^{-1}$)	Pore size (nm)	Pore volume ($cm^3\ g^{-1}$)	Pt size (nm)	Pt dispersion (%)	Acidity (mmol $NH_3/g_{cat.}$)[a]	Lewis acidity ($\mu mol/g_{cat.}$)[b]	Brønsted acidity ($\mu mol/g_{cat.}$)[b]
Pt/Al_2O_3	179.1	11.6	0.593	2.1	53.5	0.17	47.5	1.7
$Pt–5WO_x/Al_2O_3$	160.3	11.9	0.550	1.8	64.7	0.33	85.7	29.4
$Pt–10WO_x/Al_2O_3$	145.0	12.2	0.481	1.5	78.1	0.41	141.2	39.1
$Pt–15WO_x/Al_2O_3$	133.8	12.8	0.434	1.8	63.2	0.40	138.0	37.5
$Pt–20WO_x/Al_2O_3$	121.5	13.6	0.401	1.9	59.0	0.38	129.1	35.4

[a] The amount of acid sites was determined by quantifying the desorbed NH_3 from NH_3–TPD.
[b] The amount of acid sites was determined by quantifying the desorbed pyridine from Py–IR.

3. Results

3.1. Catalyst characterizations

3.1.1. Physicochemical properties of catalysts

Table 1 lists the textural properties for $Pt–WO_x/Al_2O_3$ catalysts with different WO_x loading. Only a minor decrease in surface area was observed with an increase in WO_x content. The Pt particle size and dispersion can be determined by measuring the amount of CO adsorbed because CO is adsorbed more preferentially on the surface of Pt atoms than of WO_x species at room temperature [31]. As shown in Table 1, the irreversible CO uptake was an indication of Pt dispersion of 53.5% for Pt/Al_2O_3 catalyst. Despite good Pt dispersion in Pt/Al_2O_3, it still enhanced with the increasing WO_x loading up to 10 wt%, implying that WO_x species had positive impact on the dispersion of Pt. However, further increase in WO_x content declined the dispersion mildly. Such a decrease in Pt dispersion was virtually not ascribed to the change in Pt particles sizes, which may originate from partial blockage of Pt sites by excessive WO_x species. Similar coverage effects have been widely reported in the cases of ReO_x [32], SnO_x [33], and MoO_x [34]. This can be explained by the double effects of WO_x promoter, namely bimetallic coverage effect and dispersion effect. Previous research on $Ru–MoO_x/ZrO_2$ has confirmed that the presence of minor MoO_x species promotes the dispersion of Ru sites, while redundant MoO_x can weaken the dispersion effect and cover Ru sites [34].

Fig. 1a and c displays representative HRTEM images of reduced Pt/Al_2O_3 and $Pt–10WO_x/Al_2O_3$. The dispersed Pt nanoparticles were surrounded by acicular γ-Al_2O_3 for these two samples, which can be clearly verified by the lattice fringes of Pt (d = 0.223 nm) [35]. Addition of WO_x to Pt/Al_2O_3 moderately enhanced Pt dispersion and declined Pt particle size correspondingly (Fig. 1b and d). As shown in the size distribution histogram of $Pt–10WO_x/Al_2O_3$, most of Pt nanoparticles are in the range of 0.8–2.0 nm, and no particles larger 3 nm were detected. Notably, no concrete evidence pointed to the formation of WO_x clusters over $Pt–10WO_x/Al_2O_3$, speculating that the TEM-invisible WO_x species primarily existed as polytungstate (see below).

The XRD patterns of $Pt–WO_x/Al_2O_3$ catalysts with various WO_x loading are displayed in Fig. 2. The diffraction lines at 37.4°, 46.0° and 67.0° were attributed to support γ-Al_2O_3 [14]. For catalysts with WO_x loading lower than 10 wt%, the absence of any diffrac-

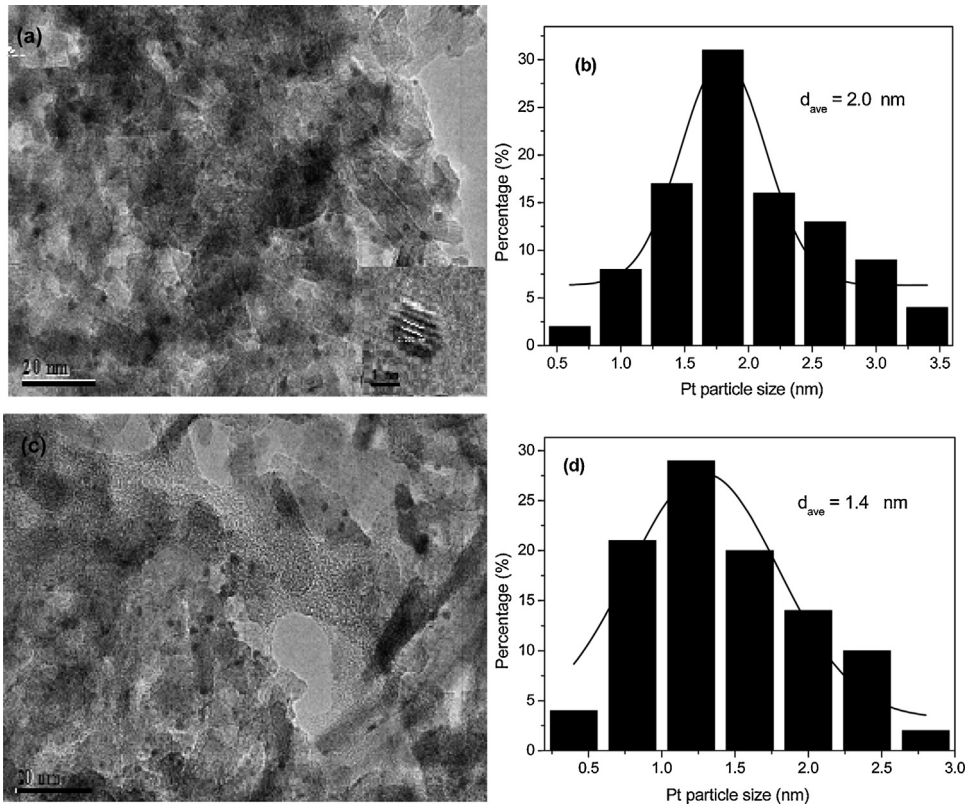

Fig. 1. HRTEM images of reduced (a) Pt/Al_2O_3 and (c) $Pt–10WO_x/Al_2O_3$ with Pt particle size distribution of (b) Pt/Al_2O_3 and (d) $Pt–10WO_x/Al_2O_3$.

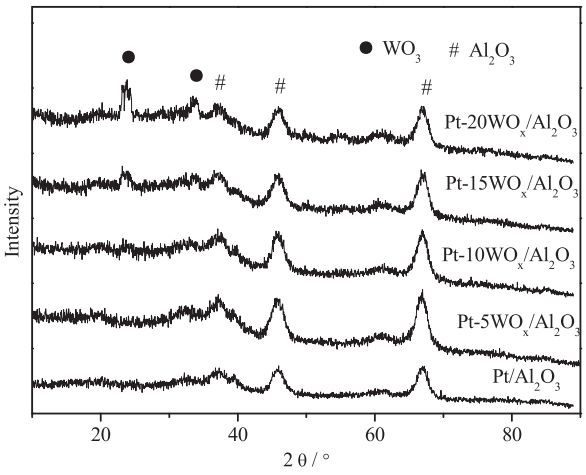

Fig. 2. XRD patterns of Pt/Al_2O_3 and $Pt–WO_x/Al_2O_3$ catalysts.

tion peaks related to WO_x species was detected, implying the homogenous dispersion of WO_x species on the Al_2O_3 surface. However, further increase in WO_x loading improved polymerization of tungstic species and resulted in the formation of monoclinic m-WO_3 (23.6° and 33.5°) [36]. The intensity of XRD diffraction peaks for m-WO_3 increased obviously with the increasing WO_x loading. It can be reasonably inferred that $Pt–10WO_x/Al_2O_3$ should be the sample with dispersion threshold of WO_x, namely reaching submonolayer coverage [36]. On the other hand, no diffraction peaks of Pt were observed, reflecting that Pt clusters were uniformly dispersed on the support surface, in agreement with CO chemisorption and TEM results. Moreover, *in situ* XRD (Fig. S1 and Fig. S2) results verified that the Pt/Al_2O_3 and $Pt–10WO_x/Al_2O_3$ catalysts were pretty stable upon high temperature treatment.

Raman spectroscopy is well-known to be suitable for examining the surface structure of WO_x species. As illustrated in Fig. 3, the Raman spectra of Pt/Al_2O_3 displayed two typical bands at 369 and 562 cm^{-1} ascribed to the γ-Al_2O_3 [37]. All these $Pt–WO_x/Al_2O_3$ samples gave a broad band at about 972–995 cm^{-1} corresponding to the stretch mode of surface monooxo W=O species [37]. Furthermore, this band shifted from 972 cm^{-1} to 995 cm^{-1} with increasing WO_x loading, suggesting the increase of WO_x domain size, namely, transformation from isolated monotungstate to polytungstate species and further aggregation to m-WO_3 clusters [36,38]. It has been identified and attributed Raman characteristic

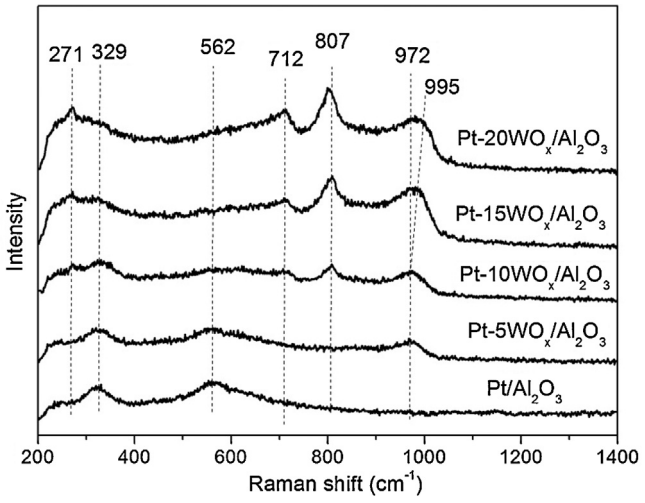

Fig. 3. Raman spectra of Pt/Al_2O_3 and $Pt–WO_x/Al_2O_3$ catalysts.

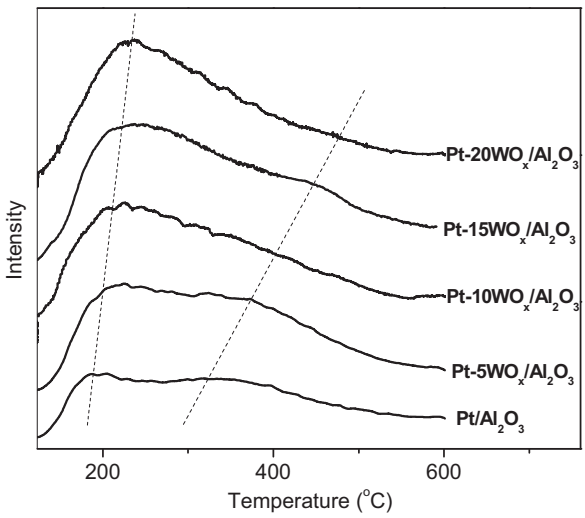

Fig. 4. NH_3–TPD profiles of Pt/Al_2O_3 and $Pt–WO_x/Al_2O_3$ catalysts.

bands at 271, 712 and 807 cm^{-1} to crystalline m-WO_3 phase [31]. Apparently, no crystalline m-WO_3 bands were detected for these catalysts below the dispersion threshold (10 wt%). These characteristic bands emerged at $Pt–10WO_x/Al_2O_3$ and then became intensive with an increase in WO_x content, in support of the XRD results.

3.1.2. Acidic properties of catalysts

The NH_3-TPD technique was employed to probe the available surface acidic sites for $Pt–WO_x/Al_2O_3$ catalysts, together with acidic strength. As displayed in Fig. 4, all the catalysts presented broad TPD profiles, reflecting that the surface acid strength was widely distributed. The NH_3–TPD profile of Pt/Al_2O_3 catalyst exhibited poorly resolved desorption peaks in two distinct temperature regions, centering at *ca.* 187 and 324 °C, which was ascribed to weak and moderate acidic sites, respectively [29]. These peaks shifted toward higher temperature and improved with increasing WO_x content, reflecting that addition of WO_x facilitated to increase acidic strength. The total acidity can be calculated on the basis of NH_3 injection experiment and the amount of acidic sites is summarized in Table 1. The total acidity enhanced continuously with the increasing WO_x loading, maximized on $Pt–10WO_x/Al_2O_3$ and then did not change the acid site distribution any more.

According to earlier study on WO_x/ZrO_2 [36,38], the acid sites improved steadily with increasing WO_x loading and attained maximum at the monolayer coverage (dispersion threshold). The surface monotungstate species at low WO_x content showed small acidity while the polytungstate became dominant at the monolayer WO_x coverage and possessed strong acid sites due to the generation of interconnected WO_x species. Nevertheless, further increase in WO_x loading led to the formation of crystalline m-WO_3 phase, which made no contribution to the total acidity. Consequently, the 10 wt% WO_x loading reached dispersion threshold and obtained the maximum acidity, consistent well with the results from XRD and Raman.

FTIR spectra of pyridine adsorption were exhibited to determine the nature of acid sites. As illustrated in Fig. 5, the bands centered at ca. 1445 and 1610 cm^{-1} were typical pyridine bands coordinated to Lewis sites [27]. The bands at *ca.* 1540 and 1640 cm^{-1} were attributed to pyridine adsorbed at Brønsted acid sites. The adsorption around 1489 cm^{-1} was assigned to the combined contribution of pyridine adsorbed on Lewis and Brønsted acid sites [10]. The concentration of Lewis and Brønsted acid sites was calculated from the integrated area of adsorption bands at *ca.* 1450 and 1540 cm^{-1}, respectively. As displayed in Table 1, Pt/Al_2O_3 pos-

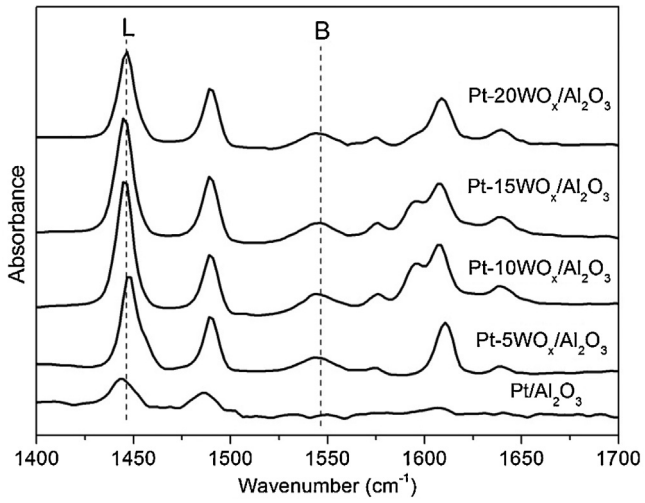

Fig. 5. FTIR spectra of pyridine adsorption of Pt/Al_2O_3 and $Pt–WO_x/Al_2O_3$ catalysts.

sessed some Lewis acid sites and hardly contained Brønsted acid sites. Addition of WO_x led to a noticeable increase in both Lewis and Brønsted acid sites. Triwahyono et al. [39] suggested that Brønsted acid sites were stemmed from surface OH groups bonded on the exposed or well-dispersed WO_x of WO_3/ZrO_2 while Lewis acid sites were generated by the removal of surface OH groups. As a result, $Pt–10WO_x/Al_2O_3$ existed as surface monolayer WO_x coverage and exposed the most surface WO_x species, resulting in the highest acid sites in terms of Lewis and Brønsted acid sites, in agreement with NH_3–TPD results.

3.1.3. Reducibility property and chemical state

Fig. 6 displays the H_2–TPR profiles of Pt/Al_2O_3 and $Pt–WO_x/Al_2O_3$ catalysts. Pt/Al_2O_3 showed a broad PtO_x reduction at around 155 °C, in line with the previous report [40]. The incorporation of WO_x remarkably decreased the reduction temperature of PtO_x because of the strong electron interaction between PtO_x and

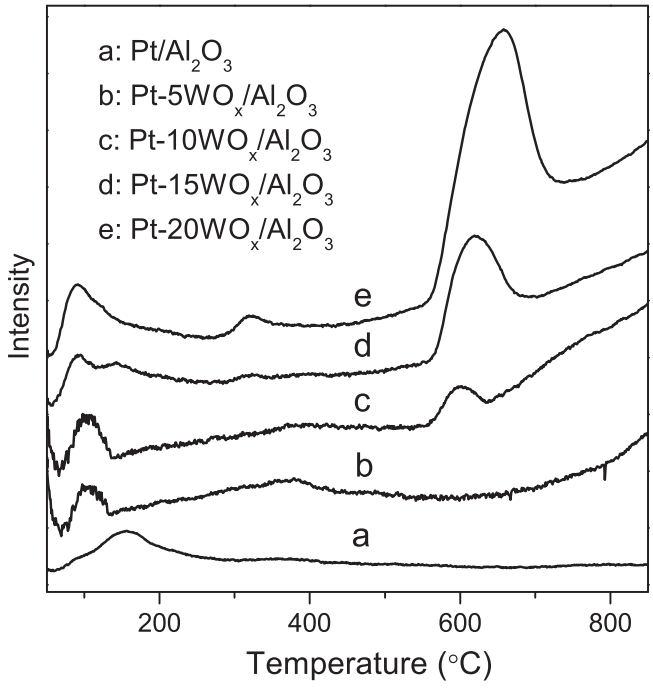

Fig. 6. H_2–TPR profiles of Pt/Al_2O_3 and $Pt–WO_x/Al_2O_3$ catalysts.

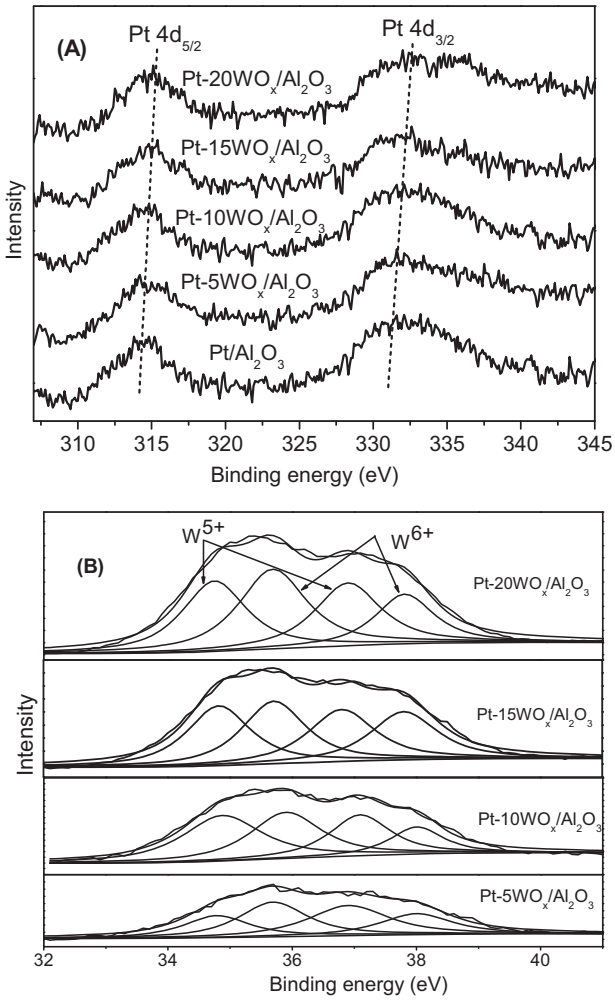

Fig. 7. (A) Pt 4d and W4f (B) XPS photoemission peaks of reduced Pt/Al_2O_3 and $Pt–WO_x/Al_2O_3$ catalysts.

WO_x species (see below). The WO_x-containing catalysts presented other two peaks at *ca.* 320 and 620 °C, which were corresponding to the reduction of $WO_3 \rightarrow WO_{2.9}$ and $WO_{2.9} \rightarrow WO_2$, respectively [41]. There was a general enhancement in the total hydrogen consumption with the increasing WO_x loading, indicating the increasing amount of potential reducible species as WO_x loading improved.

XPS analysis is used to identify surface chemical states after reduction at 200 °C and the results are depicted in Fig. 7. The Pt 4d lines (Fig. 7A) were analyzed instead of the most intense Pt 4f lines due to their serious overlapping with the strong Al 2p peaks [33]. The two peaks at *ca.* 314.5 and 331.3 eV were ascribed to Pt $4d_{5/2}$ and Pt $4d_{3/2}$ of metallic Pt, respectively, suggesting that the surface Pt species had been reduced to zero-valent Pt completely [22]. Fig. 7B illustrates XPS spectra of W 4f consisting of two spin–orbit components. In the W 4f region, the doublet at binding energies of *ca.* 34.9 and 37.0 eV was corresponding to $W4f_{7/2}$ and W $4f_{5/2}$ of W^{5+}, and another one at 35.9 and 38.1 eV was assigned to $W4f_{7/2}$ and W $4f_{5/2}$ of W^{6+} [42]. As shown in Table S1, the Pt 4d peak position moved to higher binding energy with increasing WO_x content, while the W 4f peak shifted to lower binding energy simultaneously. The declining electron density in Pt^0 nucleus originated from the electron scavenging property of WO_x [41]. Accordingly, an electronic donor-acceptor interaction between Pt^0 and WO_x might take place on γ-Al_2O_3 surface. The above results revealed the existence of strong interaction between Pt^0 and WO_x species wherein the

electron was prone to transfer from Pt^0 to WO_x species. In addition, some partially reduced W^{5+} species were formed for all the samples. Kuba et al. [43] observed similar phenomenon in Pt–WO_x/ZrO_2 and argued that the hydrogen atoms from dissociative adsorption hydrogen molecule on Pt surface could spillover to WO_3 surface and result in its reduction.

3.1.4. Catalytic performance of Pt–WO_x/Al_2O_3

Table 2 lists the catalytic activity and product distributions for Pt–WO_x/Al_2O_3 catalysts. The Pt/Al_2O_3 catalyst exhibited poor activity; the conversion was merely 9.3%. In contrast to Pt/Al_2O_3, glycerol conversion enhanced greatly for WO_x promoted catalysts. Regarding the selectivity, 1,3-PDO selectivity on Pt/Al_2O_3 was only 9.4%, similar to the result (12.1%) reported by Delgado et al. [40]. The other products were main 1,2-PDO (67.6%), and minor 1-PO with 2-PO derived from sequential hydrogenolysis of propanediols. Conversely, with the promotion of WO_x, even in a minor amount, 1,3-PDO selectivity increased considerably. For example, the selectivity of 1,3-PDO was up to 54.3% over Pt–5WO_x/Al_2O_3, whereas that of 1,2-PDO declined to a lower level (8.4%). 1,3-PDO selectivity enhanced with increasing WO_x loading and attained a maximum at 10 wt% WO_x content with a ratio of 1,3-PDO/1,2-PDO as high as 11.6. Nevertheless, further increase in WO_x loading led to its mild decrease. Of the catalysts tested, Pt–10WO_x/Al_2O_3 achieved the excellent performance, up to 42.4% 1,3-PDO yield, which was among the best reported results [8,21–25,28]. Additionally, 1-PO selectivity improved drastically for WO_x modified Pt/Al_2O_3 catalysts while 2-PO selectivity varied slightly. This can be explained by the fact that 1,2-PDO primarily tended to proceed sequential hydrogenolysis to form 1-PO [24,29]. Taken together, addition of WO_x significantly enhanced glycerol conversion and switched the main product from 1,2-PDO to 1,3-PDO by changing the dissociation of C—O bond.

4. Discussion

4.1. The structure feature of Pt–WO_x/Al_2O_3 catalysts

It is well-known that WO_x has been extensively employed as an acidic additive, such as glycerol dehydration [44], hydrolysis of cellobiose [38] and alkane isomerization [43]. As deduced by XRD, Raman and NH_3–TPD results, the molecular structures of WO_x on Pt/Al_2O_3 catalysts consisted of monotungstate, polytungstate and crystalline WO_3 clusters, which depended on WO_x loading. The WO_x on Pt–5WO_x/Al_2O_3 primarily existed in the form of monotungstate due to its low WO_x loading in highly dispersed state on support surface. When WO_x content reached its dispersion threshold over Pt–10WO_x/Al_2O_3, namely sub-monolayer coverage, polytungstate became dominant and held the maximum acidity. Theoretical calculation also reveals that at monolayer coverage octahedral polytungstate species has the most abundant edge sites owing to condensation process, and the edge sites are the most acidic units [45]. The superfluous WO_x in Pt–15WO_x/Al_2O_3 and Pt–20WO_x/Al_2O_3 existed as crystalline WO_3 phase that made no contribution to the number of acid sites.

XPS results indicated that the interaction between Pt and WO_x diminished the electron density of Pt, which was stemmed from the scavenging property of WO_x. The interaction also enhanced the reducibility of PtO_x, and increased dispersion of Pt for WO_x promoted Pt/Al_2O_3 catalysts. TEM and CO-chemisorption results confirmed that Pt dispersion of Pt–WO_x/Al_2O_3 was high, with only some detectable nanoclusters. Moreover, the deficient electron density of Pt sites facilitates to adsorb H_2 and promotes their dissociation, essential for the hydrogenation of intermediates in glycerol hydrogenolysis. The electron transfer enhances electron density of WO_x and results in promoting the protonation of hydroxyl group of glycerol via withdrawing electrons from the oxygen atom in its hydroxyl group [46]. Such enhanced protonation favors glycerol dehydration to form intermediate. In sum, compared to Pt/Al_2O_3, this electron effect between Pt and WO_x species is instrumental in elevating the catalytic behavior of glycerol hydrogenolysis for Pt–WO_x/Al_2O_3.

As PtO_x is reduced to Pt by H_2, it is speculated that H_2 spillover can occur in glycerol hydrogenolysis for Pt–WO_x/Al_2O_3. H_2 molecule can dissociative chemisorb on Pt sites and the formed hydrogen atoms tend to spillover to the nearby WO_3 surface. These hydrogen atoms are very active and induce the partial reduction of W^{6+} to W^{5+} [43]. The formation of abundant W^{5+} species was demonstrated by XPS results. Furthermore, the “hydrogen spillover” has been well established on the basis of the reduction of Pt/WO_3 system by H_2, in which tungsten bronzes such as H_xWO_3 are formed [47]. R. Prins [48] insist that hydrogen spillover from a metal surface to the surface of non-reducible support such as Al_2O_3, SiO_2, MgO, and zeolites is energetically impossible. As a result, hydrogen spillover cannot occur over Pt/Al_2O_3 catalyst. Notably, the WO_x modified Pt/Al_2O_3 catalysts endow “hydrogen spillover” ability and lead to the formation of large amount of active hydrogen and W^{5+} species simultaneously, which should greatly enhance the reaction rate of hydrogenation of intermediates in glycerol hydrogenolysis.

4.2. Structure-behavior relationship

Production of propanediols (1,2-PDO and 1,3-PDO) from glycerol hydrogenolysis involves acid-catalyzed dehydration to form intermediates (acetol and 3-hydroxypropaldehyde (3-HPA)) and subsequent hydrogenation on metal sites [29,49–51]. Therefore, higher acid sites, metals sites and active hydrogen species are favorable to convert glycerol. The WO_x modified Pt/Al_2O_3 catalysts enhanced the total acidity, electronic interaction between Pt with WO_x and hydrogen spillover, which was responsible for their superior catalytic performance.

The nature of acid site indeed plays a key role in determining the product distribution. Brønsted acid site is prone to removal of secondary hydroxyl group of glycerol to generate 1,3-PDO while Lewis acid sites favors to form 1,2-PDO [19,52]. As shown in Fig. 8, it is evident that 1,3-PDO yield is approximately proportional to the concentration of Brønsted acid, reflecting the preferential generation of 1,3-PDO on Brønsted acid sites. Apparently, addition of WO_x species significantly improves the amount of Brønsted acid, rendering the superior 1,3-PDO selectivity. The Pt–10WO_x/Al_2O_3 catalyst in the series has the largest amount of Brønsted acid sites and exhibits the highest 1,3-PDO yield, nearly 50 times that of Pt/Al_2O_3 under the same conditions.

Regarding the relationship between 1,2-PDO yield and Lewis acid sites, the correlation is not good, which is mainly ascribed to the instability of 1,2-PDO [26,29]. Our earlier report [29] has confirmed that the formed propanols (1-PO + 2-PO) are primarily derived from sequential hydrogenolysis of 1,2-PDO in glycerol hydrogenolysis, as also elucidated on Pt–WO_x/Al_2O_3. The reaction results for hydrogenolysis of glycerol, 1,2-PDO and 1,3-PDO over Pt–10WO_x/Al_2O_3 is displayed in Table S2. The conversion of 1,3-PDO was much lower than that of 1,2-PDO and glycerol, which can explain the high 1,3-PDO selectivity in glycerol hydrogenolysis over Pt–10WO_x/Al_2O_3. Additionally, the 1-PO/2-PO ratio in glycerol hydrogenolysis was similar to that in 1,2-PDO hydrogenolysis. Thus, it is reasonably to infer that 1-PO and 2-PO are predominantly derived from 1,2-PDO in glycerol hydrogenolysis. Moreover, similar behavior has been disclosed in the cases of Pt/WO_3/ZrO_2 [24], Pt/Al_2O_3 + $H_4SiW_{12}O_{40}$ [26] and ReO_x modified Ir or Rh based catalysts [53–56]. Accordingly, the calculated 1,2-PDO yield should be

Table 2
Catalytic performance of glycerol hydrogenolysis over Pt/Al_2O_3 and $Pt–WO_x/Al_2O_3$ catalysts.[a]

Catalyst	Conversion (%)	Selectivity (%)[b]				1,3-PDO/1,2-PDO (molar ratio)	1,3-PDO yield (%)
		1,3-PDO	1,2-PDO	1-PO	2-PO		
Pt/Al_2O_3	9.3	9.4	67.6	3.7	2.9	0.14	0.87
$Pt–5WO_x/Al_2O_3$	40.4	54.3	8.4	24.6	6.5	6.5	21.9
$Pt–10WO_x/Al_2O_3$	64.2	66.1	5.7	20.3	3.7	11.6	42.4
$Pt–15WO_x/Al_2O_3$	56.0	61.2	6.5	22.7	4.3	9.4	34.3
$Pt–20WO_x/Al_2O_3$	53.4	58.9	6.0	23.1	4.0	9.8	31.5

[a] Reaction conditions: 160 °C, 5.0 MPa, H_2/glycerol = 137:1 (molar ratio), WHSV = 0.09 h^{-1}.
[b] 1,3-PDO: 1,3-propanediol, 1,2-PDO: 1,2-propanediol, 1-PO: 1-propanol, 2-PO: 2-propanol.

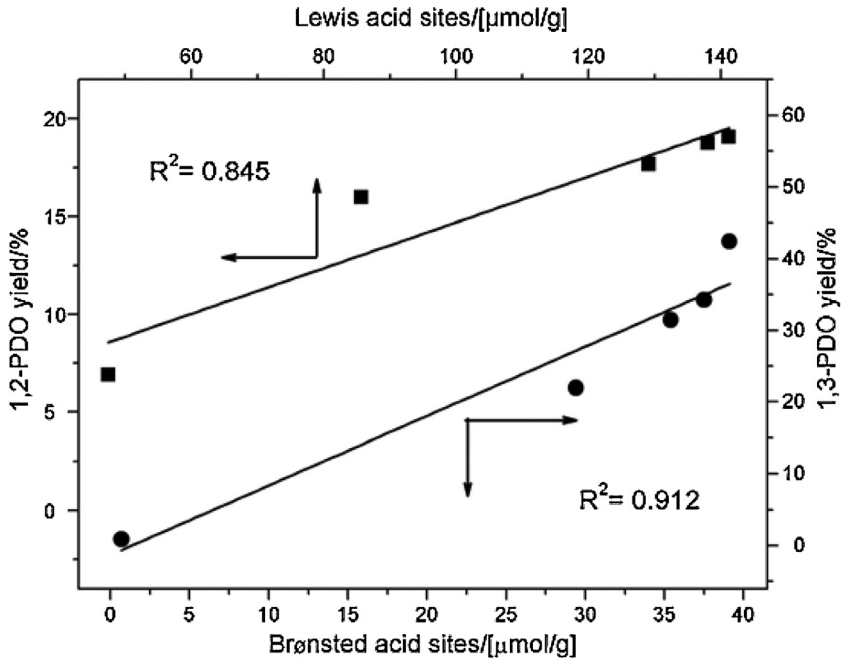

Fig. 8. Correlation between the amount of acids sites and product yield over Pt/Al_2O_3 and $Pt–WO_x/Al_2O_3$ catalysts. Reaction conditions: 160 °C, 5.0 MPa, H_2/glycerol = 137:1 (molar ratio), WHSV = 0.09 h^{-1}.

the sum of detected 1,2-PDO and the part that has been converted to propanols. Interestingly, a roughly linear correlation between the calculated 1,2-PDO yield and the concentration of Lewis acid sites is also given in Fig. 8, revealing the essential active sites of Lewis acid sites for glycerol hydrogenolysis to 1,2-PDO.

Previous reports [57–61] showed that the main product was not 1,3-PDO but 1,2-PDO when using Ru/C and Brønsted acidic Amberlyst catalyst. Because Ru/C and Amberlyst was only mixed mechanically, the formed intermediate 3-HPA in Brønsted acid sites cannot immediately hydrogenate to 1,3-PDO. Meanwhile, large amount of 1,2-PDO was produced over Ru/C due to the weak Lewis acidic sites. Compared to Ru/C alone, the main product was still 1,2-PDO over Ru/C + Amberlyst. Contrarily, the formed 3-HPA in Brønsted acid sites can be quickly converted into 1,3-PDO in interface between WO_x and Pt species over $Pt–WO_x/Al_2O_3$.

5. Conclusions

In this work, addition of WO_x to Pt/Al_2O_3 has demonstrated to be a powerful approach to tune acidic properties with electronic structure, and to control the catalytic performance in glycerol hydrogenolysis. The WO_x species has been identified as monotungstate, polytungstate, and crystalline m-WO_3 phase over $Pt–WO_x/Al_2O_3$ catalysts. Of the catalysts examined, $Pt–10WO_x/Al_2O_3$ attained the superior 1,3-propanediol yield up to 42.4%, nearly 50 times that of Pt/Al_2O_3, which was attributed to the abundant Brønsted acid sites, strong electronic interaction between Pt with WO_x, and hydrogen spillover.

The amount of Brønsted acid sites is proportional to 1,3-PDO yield, giving direct evidence that Brønsted acid sites facilitate to cleave secondary C—O bond of glycerol to produce 1,3-PDO. Meanwhile, the linear correlation between Lewis acid sites with 1,2-PDO yield confirms the importance of Lewis acid sites in controlling cleavage primary C—O bond to form 1,2-PDO. Accordingly, these correlations will provide guidance for designing effective catalysts to produce 1,2-PDO and 1,3-PDO, selectively.

Acknowledgements

The authors gratefully acknowledge financial support from the Major State Basic Research Development Program of China (973 Program) (No. 2012CB215305) and the National Natural Science Foundation of China (No. 21403269). We also thank Dr. Shunli Hao for valuable suggestions in catalyst preparation.

Appendix A. Supplementary data

Supplementary data associated with this article can be found, in the online version, at http://dx.doi.org/10.1016/j.molcata.2014.12.021.

References

[1] J.N. Chheda, G.W. Huber, J.A. Dumesic, Angew. Chem. Int. Ed. 46 (2007) 7164–7183.
[2] A. Corma, S. Iborra, A. Velty, Chem. Rev. 107 (2007) 2411–2502.
[3] C.H.C. Zhou, J.N. Beltramini, Y.X. Fan, G.Q.M. Lu, Chem. Soc. Rev. 37 (2008) 527–549.
[4] L. Zhang, A.M. Karim, M.H. Engelhard, Z. Wei, D.L. King, Y. Wang, J. Catal. 287 (2012) 37–43.
[5] P. Lakshmanan, P.P. Upare, N.-T. Le, Y.K. Hwang, D.W. Hwang, U.H. Lee, H.R. Kim, J.-S. Chang, Appl. Catal. A 468 (2013) 260–268.
[6] W. Suprun, M. Lutecki, T. Haber, H. Papp, J. Mol. Catal. A 309 (2009) 71–78.
[7] S. Zhu, Y. Zhu, S. Hao, L. Chen, B. Zhang, Y. Li, Catal. Lett. 142 (2012) 267–274.
[8] R.V. Sharma, P. Kumar, A.K. Dalai, Appl. Catal. A 477 (2014) 147–156.
[9] S. Zhu, Y. Zhu, X. Gao, T. Mo, Y. Zhu, Y. Li, Bioresource Technol. 130 (2013) 45–51.
[10] S. Zhu, X. Gao, F. Dong, Y. Zhu, H. Zheng, Y. Li, J. Catal. 306 (2013) 155–163.
[11] A. Behr, J. Eilting, K. Irawadi, J. Leschinski, F. Lindner, Green Chem. 10 (2008) 13–30.
[12] D. Sun, Y. Yamada, S. Sato, Appl. Catal. A 475 (2014) 63–68.
[13] S.N. Delgado, D. Yap, L. Vivier, C. Especel, J. Mol. Catal. A 367 (2013) 89–98.
[14] J.B. Salazar, D.D. Falcone, H.N. Pham, A.K. Datye, F.B. Passos, R.J. Davis, Appl. Catal. A 482 (2014) 137–144.
[15] S. Zhu, X. Gao, Y. Zhu, Y. Zhu, H. Zheng, Y. Li, J. Catal. 303 (2013) 70–79.
[16] T. Kurosaka, H. Maruyama, I. Naribayashi, Y. Sasaki, Catal. Commun. 9 (2008) 1360–1363.
[17] L. Ma, D.H. He, Catal. Today 149 (2010) 148–156.
[18] O.M. Daniel, A. DeLaRiva, E.L. Kunkes, A.K. Datye, J.A. Dumesic, R.J. Davis, ChemCatChem 2 (2010) 1107–1114.
[19] J. Oh, S. Dash, H. Lee, Green Chem. 13 (2011) 2004–2007.
[20] Y. Nakagawa, Y. Shinmi, S. Koso, K. Tomishige, J. Catal. 272 (2010) 191–194.
[21] Y. Zhang, X.-C. Zhao, Y. Wang, L. Zhou, J. Zhang, J. Wang, A. Wang, T. Zhang, J. Mater. Chem. A 1 (2013) 3724–3732.
[22] J. Chaminand, L. Djakovitch, P. Gallezot, P. Marion, C. Pinel, C. Rosier, Green Chem. 6 (2004) 359–361.
[23] Y. Nakagawa, X. Ning, Y. Amada, K. Tomishige, Appl. Catal. A 433–434 (2012) 128–134.
[24] L.-Z. Qin, M.-J. Song, C.-L. Chen, Green Chem. 12 (2010) 1466–1472.
[25] R. Arundhathi, T. Mizugaki, T. Mitsudome, K. Jitsukawa, K. Kaneda, ChemSusChem 6 (2013) 1345–1347.
[26] J. Dam, K. Djanashvili, F. Kapteijn, U. Hanefeld, ChemCatChem 5 (2013) 497–505.
[27] S. Zhu, X. Gao, Y. Zhu, Y. Zhu, X. Xiang, C. Hu, Y. Li, Appl. Catal. B 140–141 (2013) 60–67.
[28] L. Gong, Y. Lu, Y. Ding, R. Lin, J. Li, W. Dong, T. Wang, W. Chen, Appl. Catal. A 390 (2010) 119–126.
[29] S. Zhu, Y. Qiu, Y. Zhu, S. Hao, H. Zheng, Y. Li, Catal. Today 212 (2013) 120–126.
[30] S. Zhu, X. Gao, Y. Zhu, J. Cui, H. Zheng, Y. Li, Appl. Catal. B 158–159 (2014) 391–399.
[31] M.N. Taylor, W. Zhou, T. Garcia, B. Solsona, A.F. Carley, C.J. Kiely, S.H. Taylor, J. Catal. 285 (2012) 103–114.
[32] Y. Amada, Y. Shinmi, S. Koso, T. Kubota, Y. Nakagawa, K. Tomishige, Appl. Catal. B 105 (2011) 117–127.
[33] T. Deng, H. Liu, Green Chem. 15 (2013) 116–124.
[34] L. Chen, Y. Zhu, H. Zheng, C. Zhang, Y. Li, Appl. Catal. 411–412 (2012) 95–104.
[35] C. Wen, Y. Zhu, Y. Ye, S. Zhang, F. Cheng, Y. Liu, P. Wang, F. Tao, ACS Nano 6 (2012) 9305–9313.
[36] K. Song, H. Zhang, Y. Zhang, Y. Tang, K. Tang, J. Catal. 299 (2013) 119–128.
[37] X. Chen, G. Clet, K. Thomas, M. Houalla, J. Catal. 273 (2010) 236–244.
[38] R. Kourieh, S. Bennici, M. Marzo, A. Gervasini, A. Auroux, Catal. Commun. 19 (2012) 119–126.
[39] S. Triwahyono, T. Yamada, H. Hattori, Appl. Catal. A 242 (2003) 101–109.
[40] S.N. Delgado, D. Yap, L. Vivier, C. Especel, J. Mol. Catal. A 367 (2013) 89–98.
[41] J.M. Grau, C.R. Vera, V.M. Benitez, J.C. Yori, Energy Fuels 22 (2008) 1680–1686.
[42] T.Y. Kim, D.S. Park, Y. Choi, J. Baek, J.R. Park, J. Yi, J. Mater. Chem. 22 (2012) 10021–10028.
[43] S. Kuba, M. Che, R.K. Grasselli, H. Knözinger, J. Phy. Chem. B 107 (2003) 3459–3463.
[44] A. Ulgen, W.F. Hoelderich, Appl. Catal. A 400 (2011) 34–38.
[45] A. Galano, G. Rodriguez-Gattorno, E. Torres-Garcia, Phys. Chem. Chem. Phys. 10 (2008) 4181–4188.
[46] M.L. Barbelli, G.F. Santori, N.N. Nichio, Bioresource Technol. 111 (2012) 500–503.
[47] Y. Xi, Q. Zhang, H. Cheng, J. Phy. Chem. C 118 (2013) 494–501.
[48] R. Prins, Chem. Rev. 112 (2012) 2714–2738.
[49] I. Gandarias, P.L. Arias, J. Requies, M.B. Guemez, J.L.G. Fierro, Appl. Catal. B 97 (2010) 248–256.
[50] M. Balaraju, V. Rekha, P.S.S. Prasad, B.L.A.P. Devi, R.B.N. Prasad, N. Lingaiah, Appl. Catal. A 354 (2009) 82–87.
[51] M.G. Musolino, L.A. Scarpino, F. Mauriello, R. Pietropaolo, ChemSusChem 4 (2011) 1143–1150.
[52] A. Alhanash, E.F. Kozhevnikova, I.V. Kozhevnikov, Appl. Catal. A 378 (2010) 11–18.
[53] Y. Amada, S. Koso, Y. Nakagawa, K. Tomishige, ChemSusChem 3 (2010) 728–736.
[54] S. Koso, H. Watanabe, K. Okumura, Y. Nakagawa, K. Tomishige, Appl. Catal. B 111–112 (2012) 27–37.
[55] Y. Shinmi, S. Koso, T. Kubota, Y. Nakagawa, K. Tomishige, Appl. Catal. B 94 (2010) 318–326.
[56] Y. Nakagawa, M. Tamura, K. Tomishige, J. Mater. Chem. A 2 (2014) 6688–6702.
[57] Y. Kusunoki, T. Miyazawa, K. Kunimori, K. Tomishige, Catal. Commun. 6 (2005) 645–649.
[58] T. Miyazawa, S. Koso, K. Kunimori, K. Tomishige, Appl. Catal. A 329 (2007) 30–35.
[59] T. Miyazawa, S. Koso, K. Kunimori, K. Tomishige, Appl. Catal. A 318 (2007) 244–251.
[60] I. Furikado, T. Miyazawa, S. Koso, A. Shimao, K. Kunimori, K. Tomishige, Green Chem. 9 (2007) 582–588.
[61] T. Miyazawa, Y. Kusunoki, K. Kunimori, K. Tomishige, J. Catal. 240 (2006) 213–221.